Journal of Alloys and Compounds 509 (2011) 2060–2065

Contents lists available at ScienceDirect

Journal of Alloys and Compounds

journal homepage: www.elsevier.com/locate/jallcom

# A simple method to prepare $Ln(OH)_3$ (Ln = La, Sm, Tb, Eu, and Gd) nanorods using CTAB micelle solution and their room temperature photoluminescence properties

Qiuying Mu, Yude Wang*

*Department of Materials Science and Engineering, Yunnan University, Kunming 650091, People's Republic of China*

ARTICLE INFO

*Article history:*
Received 2 September 2010
Received in revised form 22 October 2010
Accepted 28 October 2010
Available online 4 November 2010

*Keywords:*
Surfactant-mediated method
Rare-earth hydroxides
Nanorods
Room temperature photoluminescence

ABSTRACT

The stable and crystalline pure phase $Ln(OH)_3$ (Ln = La, Sm, Tb, Eu, and Gd) nanorods with diameters of approximately 15–90 nm and lengths of 120–500 nm were synthesized using cationic surfactant (cetyltrimethylammonium bromide, CTAB) micelle solution at room temperature. X-ray diffraction (XRD) spectra, Fourier transformed infrared (FTIR) spectrum, transmission electron microscopy (TEM), high-resolution TEM (HRTEM) and Raman spectroscopy were used to examine the morphologies and microstructures to find out the cause. The four observed Raman peaks indicated the typical hexagonal phase, which was in agreement with the X-ray diffraction results. A possible formation mechanism of these $Ln(OH)_3$ nanorods was proposed. The results suggest that this process may be a convenient and effective approach to prepare rare-earth hydroxides with 1D nanostructures. Room temperature photoluminescence (RTPL) properties were investigated under the excitation of 275 nm. The samples exhibited the emission peaks of room temperature photoluminescence.



## 1. Introduction

One-dimensional (1D) nanostructures, such as nanowires, nanobelts, nanotubes, and nanorods were prepared and used in a lot of fields. Owing to their unique physical and chemical properties, they were thus expected to be critical to the function and integration of nanoscale devices [1]. Very recently, much attention has been paid to the preparation and optical property. In fact, rare-earth compounds are an important family of inorganic material that have been widely used as luminescent devices, catalysts, magnet materials, fluorescence labels for biological detection, and other functional materials based on the electronic, optical, and chemical characteristics resulting from their unique 4f electron configuration [2–6]. As those properties within the nanometer regime might be associated with their morphologies, thus if rare-earth oxides were fabricated in the form of a 1D nanostructure, they would hold promise as highly functionalized materials as a result of both shape-specific and quantum confinement effects. Rare-earth hydroxides are of great importance because they represent a straightforward approach toward oxides or sulfides through dehydration or sulfuration. Hydroxyl groups may also act as active sites for surface grafting through condensation reactions of organic and/or biological reagents [7]. Because of its advantages, the role of chemistry in materials science has been rapidly growing. Very recently, much attention has been paid to the preparation and optical property study of rare-earth hydroxide one-dimensional nanostructures [8–11]. The chemical methods were adopted for the preparation of rare-earth hydroxide nanostructures including hydrothermal [8,11], microwave technique [9], wet-chemical approach [10], solvothermal [12], hydrothermal microemulsion [13], and composite-hydroxide-mediated (CHM) [14]. The synthesis of these nanostructures is based on the preparation of rare-earth hydroxide colloidal precipitates and the subsequent hydrothermal treatment at a designated temperature. The nanostructure morphologies were tuned by changing experimental parameters. Among them, the hydrothermal method is widely used to prepare the nanostructural materials because of its simplicity, high efficiency, and low cost. However, the hydrothermal synthesis technology was somewhat difficult for industrial production. To our knowledge, the development of facile, economical and effective methods for rare-earth hydroxides nanostructures remains a challenge due to a limited understanding of the formation mechanism of different rare-earth hydroxides morphologies. It is also necessary to explore a new, low-temperature and low-cost synthesis method for nanostructured rare-earth hydroxides for its applications. Here, we report a simple and new method for direct growth of the rare-earth hydroxides nanorods with no post-annealing from the simple chemical reagents (hydrous rare-earth chloride ($LnCl_3 \cdot 6H_2O$, Ln = La, Sm, Tb, Eu, and Gd) and $NH_3 \cdot H_2O$) at room temperature. In this approach, the cations (rare-earth) are assembled within the template of surfactant micelle in an aqueous solution. The surfactant not only provides favorable site for the

* Corresponding author. Tel.: +86 0871 5031124; fax: +86 0871 5031124.
*E-mail address:* ydwang@ynu.edu.cn (Y. Wang).

0925-8388/$ – see front matter © 2010 Elsevier B.V. All rights reserved.
doi:10.1016/j.jallcom.2010.10.141

growth of the particulate assemblies, it also influences the formation process, including nucleation, growth, coagulation, and flocculation [15]. Surfactant plays an important role in the preparation of $Ln(OH)_3$ nanorods. $Ln(OH)_3$ nanorods with the different length–diameter ratios have been successfully prepared. In addition, the room temperature photoluminescence properties are also investigated.

## 2. Materials and methods

### 2.1. Synthesis of rare-earth hydroxide nanorods

All chemical reagents used in the experiments were obtained from commercial sources as guaranteed-grade reagents and used without further purification. The purity of CTAB was 99% and the purities of the inorganic precursors were not less than 99.90% respectively.

The synthesis of rare-earth hydroxide ($Ln(OH)_3$, Ln = La, Sm, Tb, Eu, and Gd) nanorods was based on the cationic surfactant (CTAB) and the simple chemical materials (rare-earth chloride hexahydrate $LnCl_3{\cdot}6H_2O$ and $NH_3{\cdot}H_2O$) as inorganic precursors. The synthesis processes were carried out at room temperature. In a typical process, the synthesis procedure is as follows: The CTAB (6 mmol) was dissolved in distilled water (20 ml) with slowly stirring for several minutes until a clear homogeneous solution was obtained. The $LnCl_3{\cdot}6H_2O$ (4 mmol) was mixed with distilled water (10 ml) until a homogenous solution was obtained. The solution of $LnCl_3{\cdot}6H_2O$ was then added into the obtained CTAB solution with stirring. After stirring 30 min, the mixing solution became homogeneous, a solution of diluted $NH_3{\cdot}H_2O$ (25–28 wt% solution, 48 ml) was added into with vigorous stirring. Precipitates of $Ln(OH)_3$ appeared immediately. Then the above mixing solution was stirred for 2 h at room temperature. The products had been aged at ambient temperature for one month. The final products were collected by filtering, washing with distilled water to remove surfactant and then dried in an oven at 60 °C.

### 2.2. Characterization of rare-earth hydroxide nanorods

X-ray diffraction (XRD) patterns were recorded in reflection mode (Cu Kα radiation) on a Bruker D8 diffractometer. FTIR spectra were recorded using a Varian 600 FTIR Spectometer. Before each measurement, the background spectrum was taken and subtracted from the FTIR spectrum of the samples. The rare-earth hydroxide nanorods were characterized using an Omega 912 transmission electron microscope (TEM) (Carl Zeiss, Oberkochen, Germany) at an acceleration voltage of 120 kV, while high-resolution transmission electron microscopy (HRTEM) characterization was done using JEOL JEM-2010 Electron Microscope (with an acceleration voltage of 200 kV). The samples for TEM were prepared by dispersing the final samples in distilled water, this dispersing was then dropped on carbon–copper grids covered by an amorphous carbon film. To prevent agglomeration of nanorods the copper grid was placed on a filter paper at the bottom of a Petri dish. The Raman spectra were recorded with a Renishaw inVia Raman microscope, equipped with a CCD (charge coupled device) with the detector cooled to about 153 K using liquid $N_2$. The laser power was set at 300 mW. The spectral resolution was 1 $cm^{-1}$. UV–vis measurements were made with a UV-2401PC spectrophotometer. Room temperature photoluminescence (RTPL) experiments were measured on a Hitachi F-4500 FL spectrophotometer using a Xenon lamp as the excitation source at room temperature. All experiments were performed at room temperature.

## 3. Results and discussion

The typical XRD pattern in Fig. 1 can be readily indexed to a pure hexagonal phase [space group: $P6_3/m$ (176)]. All diffraction peaks can be perfectly indexed to $Ln(OH)_3$, and are in good agreement with the values in the corresponding JCPDS standard cards $La(OH)_3$ (JCPDS No. 36-1481), $Eu(OH)_3$ (JCPDS No. 83-2305), $Tb(OH)_3$ (JCPDS No. 19-1325), $Gd(OH)_3$ (JCPDS No. 83-2037), and

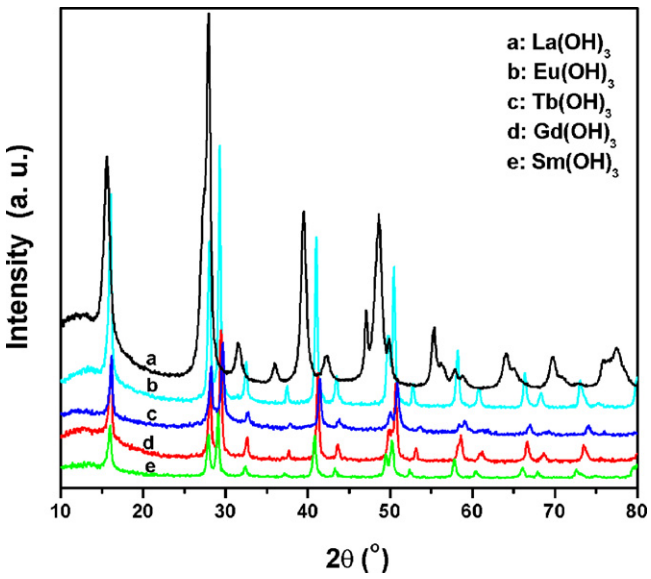


**Fig. 1.** X-ray diffraction analysis of $Ln(OH)_3$ nanorods.

$Sm(OH)_3$ (JCPDS No. 83-2036). The materials show well-developed diffraction lines of rare-earth hydroxides without any indication of crystalline byproducts such as $LnCl_3$ or CTAB. No impurity peaks are observed, indicating the high purity of the products. The lattice constants of the products are presented in Table 1.

The rare-earth hydroxides have the same hexagonal structure as the lighter rare-earth chlorides ($C_{6h}^2$, $P6_3/m$), with the OH dipoles replacing the $Cl^-$ ions and with the dipole axis lying in the mirror planes perpendicular to the crystal hexagonal axis. The crystal structure character of $Ln(OH)_3$ (Ln = Eu, Sm) has been studied by Xu et al. [16]. The structure of $Ln(OH)_3$ is represented that the Ln atoms are placed in positional set 2(c) with a special site (1/3, 2/3, 1/4), and the oxygen atoms are placed in positional set 6(h) with a special site ($x$, $y$, 1/4). $Ln(OH)_3$ nanorods crystal structure is similar to that of ZnO [17] and $LnPO_4$ [18]. The crystal structure of the representative hexagonal $Ln(OH)_3$ is shown in Fig. 2. According to the crystal structure character of $Ln(OH)_3$, the atomic interactions along the *a*- and *b*-directions are much weaker than that along the *c*-axis, this means that the growth direction of the $Ln(OH)_3$ nanostructures is largely confined to the [0 0 1] direction [16].

The fabricated $Ln(OH)_3$ materials were characterized by spectroscopic techniques. Some bands attributed to CTAB surfactant are not observed in the region 2800–3020 $cm^{-1}$ from Fig. 3. The asymmetric (2918.7 $cm^{-1}$) and symmetric (2846.4 $cm^{-1}$) stretching vibrations of $C–CH_2$ and $C–CH_3$ asymmetric stretching and $N–CH_3$ symmetric stretching vibrations (3011.6 $cm^{-1}$) are assigned to solid surfactant CTAB. For the as-synthesized $Ln(OH)_3$ nanorods, the inexistence of $CH_2$ vibrations at 2846.4 and 2918.7 $cm^{-1}$ indicates that the surfactant is not present in the as-synthesized sample. In addition to the band at 600–750 $cm^{-1}$, which is due to the bend vibration of Ln–O–H, the FTIR spectra (Fig. 3) of an

**Table 1**
The phase structures and lattice constants of $Ln(OH)_3$ nanorods.

| $Ln(OH)_3$ | ICDD PDF no. | JCPDS | | Average lattice constants | | Average diameter/length (nm) |
|---|---|---|---|---|---|---|
| | | $a$ (Å) | $c$ (Å) | $a$ (Å) | $c$ (Å) | |
| $La(OH)_3$ | 36-1481 | 6.528 | 3.858 | 6.568 | 3.831 | 10/150 |
| $Eu(OH)_3$ | 83-2305 | 6.352 | 3.653 | 6.430 | 3.596 | 30/500 |
| $Tb(OH)_3$ | 19-1325 | 6.312 | 3.601 | 6.341 | 3.570 | 20/400 |
| $Gd(OH)_3$ | 83-2037 | 6.329 | 3.631 | 6.341 | 3.632 | 15/500 |
| $Sm(OH)_3$ | 83-2036 | 6.368 | 3.683 | 6.386 | 3.863 | 15/300 |

The average lattice constants were calculated from (1 0 0), (1 1 0), (1 0 1), (2 0 1), (2 1 1), and (1 1 2) reflections based on the experimental data.

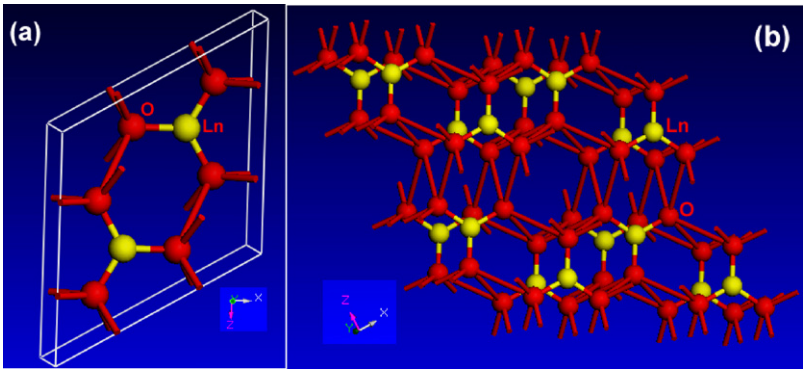


**Fig. 2.** The crystal structure of hexagonal $Ln(OH)_3$ (a) and of viewed from the *y*-axis (b).

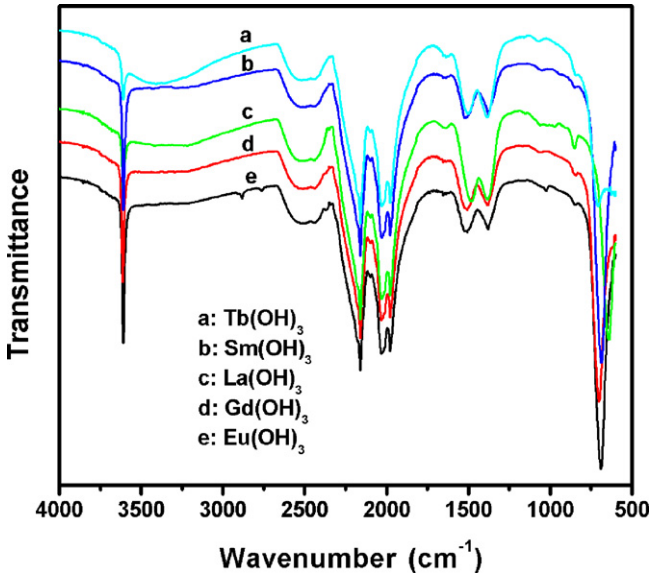


**Fig. 3.** FTIR spectra of $Ln(OH)_3$ nanorods.

as-prepared samples display three strong absorption bands at wavenumbers of 1300–1500, 1900–2100, and 2200–2300 $cm^{-1}$. An intense and sharp band at 3609.4 $cm^{-1}$ is assigned to the stretching and bending O–H vibrations of rare-earth hydroxides. The bands at 3421.4 $cm^{-1}$ and 1631.3 $cm^{-1}$ can be attributed to the O–H vibration in absorbed water on the sample surface [19]. The FTIR spectra of the neat nanorods are similar to that of $Y(OH)_3$ nanotubes [20] and $Eu(OH)_3$ nanorods [21]. These bands fingerprint the crystal space group of the nanorods as pure hexagonal $P6_3/m$.

The morphology and structure of the products were further examined with transmission electron microscopy (TEM) and HRTEM. The $La(OH)_3$, sample is mainly composed of uniform short nanorods with diameters of about 10 nm and lengths of 100–150 nm (Fig. 4(a)). The $Sm(OH)_3$, $Gd(OH)_3$, $Eu(OH)_3$, and $Tb(OH)_3$ samples entirely consist of well-dispersed nanorods with high aspect ratios (Fig. 4(d, g, j and m)). TEM observation revealed that they all exhibited one-dimensional rod-like nanostructures of hexagonal structure. The selected-area electron diffraction (SAED) patterns of $Ln(OH)_3$ nanorods presented in Fig. 4(b, e, h, k and n) show the characteristic diffraction rings, which correspond to the reflections (1 0 1), (2 0 1), (2 1 1), and (1 1 2) of hexagonal structure. The structures of the individual nanorods were further examined by HRTEM. The HRTEM images also reveal that the surface of the nanorods is not smooth. In the parts of Fig. 4(c, f, i, l and o) close to the nanorod edge, microtwins are clearly visible. In hexagonal crystal systems and in particular in the case of a one-dimensional particle morphology (nanofibers, nanobelts, nanotubes or nanowires) there is a high probability that twins and stacking faults exist [22–24]. Their presence here and in more general the presence of planar defects within nanorods imply that nanorods growth occurred from several nucleation centers resulting in anisotropic defective structure similar as in the case of mesocrystals formation [25]. HRTEM images recorded from other areas of the samples also confirm the presence of such defect features.

The formation of a hexagonal structure of $Ln(OH)_3$ nanorods was further supported by Raman spectra. Fig. 5 presents the Raman spectra of the rare-earth hydroxide nanorods for the 150–650 $cm^{-1}$ region. $Ln(OH)_3$ are hexagonal, space group $P6_3/m$. The phonons can be classified according to $2A_{1g}$, $3A_{2u}$, $2E_g$, and $3E_u$. Four Raman active phonons ($2A_{2u}$ and $2E_u$) should be expected. In this case, the spectra of $Ln(OH)_3$ exhibit only three bands and are listed in Table 2. Librational and translational modes can be found in adjacent frequency regions both below 500 $cm^{-1}$ [26]. For the Raman scattering of $Ln(OH)_3$ nanorods, the peaks show vibration modes of Ln–O and O–H bonds in the high-frequency region (more than 3000 $cm^{-1}$). The frequencies of these bands are in agreement with the X-ray diffraction results and those reported for crystalline $Ln(OH)_3$ [26–29].

The simple chemical reaction for the precipitation of $Ln(OH)_3$ is proposed as follows:

$$Ln^{3+} + 3OH^- \rightarrow Ln(OH)_3 \quad (1)$$

Template-based systems are frequently used to control nucleation and growth of inorganic particles. In this approach, the template simply serves as a scaffold with (or around) which different materials are generated in situ and shaped into a nanostructure with its morphology complementary to that of the template. When the solutions (CTAB and $LnCl_3{\cdot}6H_2O$ mixed solution and $NH_3{\cdot}H_2O$ solution) were mixed, the white precipitate appeared at once and gradually increased with the adding of $NH_3{\cdot}H_2O$ solution, which

**Table 2**
Raman shift ($cm^{-1}$) and assignments of Raman active optical phonons in $Ln(OH)_3$ at $T = 153$ K.

| $La(OH)_3$ | $Gd(OH)_3$ | $Tb(OH)_3$ | $Eu(OH)_3$ | $Sm(OH)_3$ | Assignment |
|---|---|---|---|---|---|
| 281 | 306 | 306 | 301 | 301 | $A_g$; translatory modes predominantly of the anions |
| 336 | 385 | 391 | 376 | 374 | $E_{2g}$; translatory modes predominantly of the anions |
| 451 | 488 | 497 | 482 | 478 | $E_{1g}$; libration |

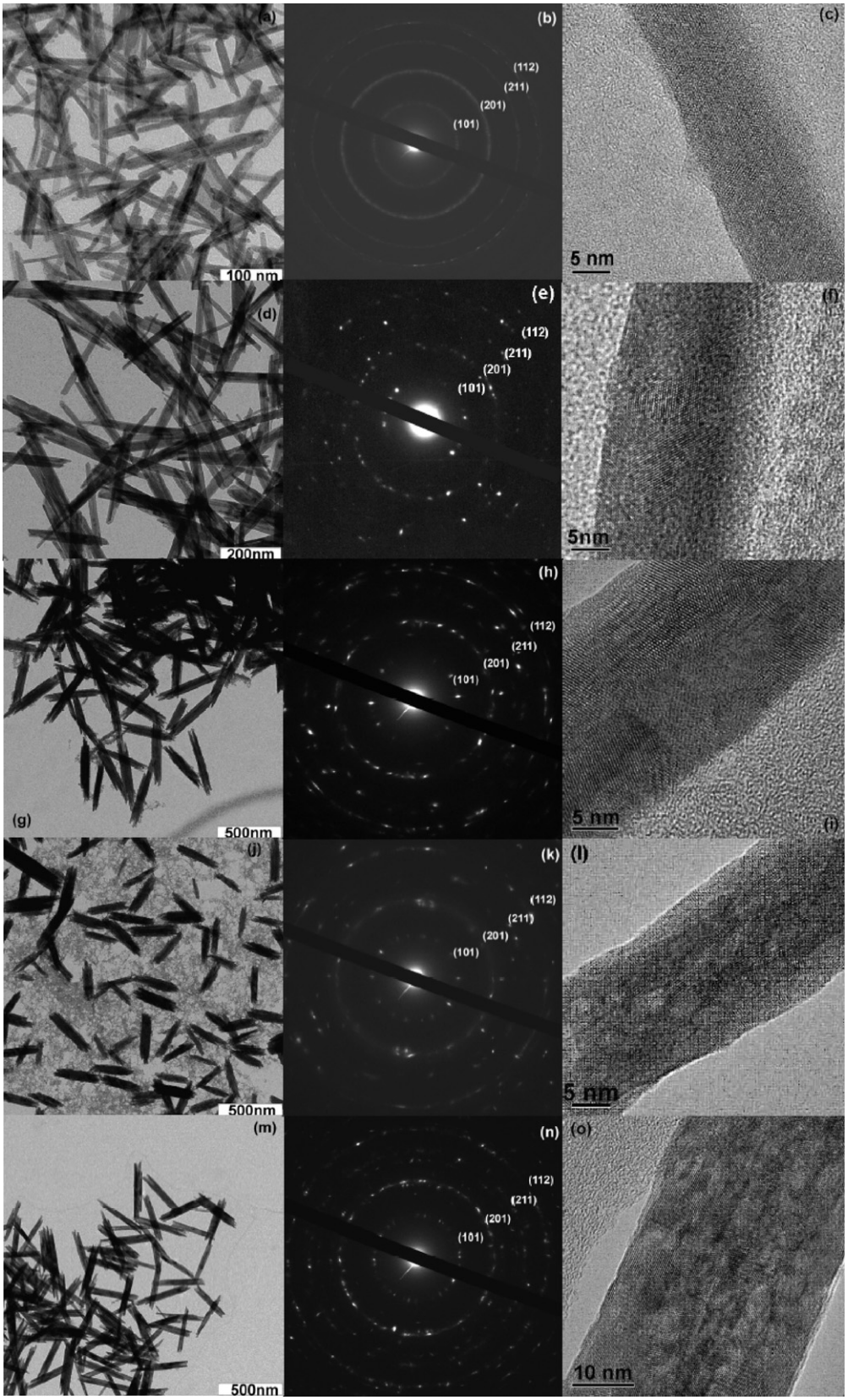


**Fig. 4.** TEM images, selected area electron diffraction, and HRTEM images of $Ln(OH)_3$ nanorods. (a)–(c): $La(OH)_3$, (d)–(f): $Sm(OH)_3$, (g)–(i): $Gd(OH)_3$, (j)–(l): $Tb(OH)_3$, and (m)–(o): $Eu(OH)_3$.

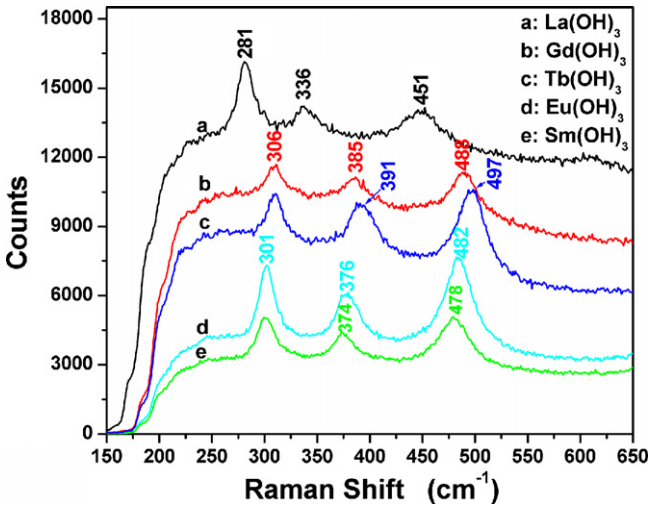


**Fig. 5.** Raman spectrum of $Ln(OH)_3$ nanorods.

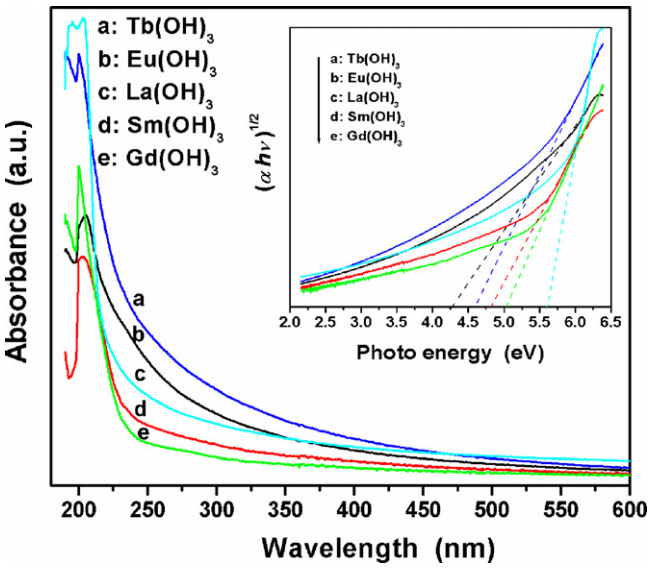


**Fig. 7.** Absorption spectra of $Ln(OH)_3$ nanorods. Inset: apparent energy gap of $Ln(OH)_3$ nanorods from the extrapolation of Urbach's equation.

indicated that the reaction happened. On the basis of the series of experimental data, the overall assembly behaviors of the $Ln(OH)_3$ nanorods at room temperature could be illustrated as in Fig. 6. The similar formation mechanisms were reported and the generating 1D nanostructures in relatively large quantities can be synthesized by templating against rod-like micelles assembled from CTAB [30–34]. In this case, the formation of the $Ln(OH)_3$ nanorods belongs to a self-assembly process.

In recent years, the search of new rare-earth luminescent materials has received great attention, since new luminescent materials may have the capacity to solve existing problems. In order to improve the material properties, it is generally required to use nanostructures with controlled shape and size as starting materials. Designing systems with lower dimensionality like nanofibers, nanowires, nanobelts or nanorods is of great importance due to the possible novel properties induced by the reduced dimensionality [35]. UV–vis spectroscopy was used to characterize the optical absorbance of the $Ln(OH)_3$ nanorods. The absorption spectra of $Ln(OH)_3$ nanorods were carried out to resolve the excitonic or interband (valence-conduction band) transition of $Ln(OH)_3$ nanorods, which allows us to calculate the bandgap. The UV–vis absorption spectra of $Ln(OH)_3$ nanorods show a strong band edge absorption in the region under 250 nm (Fig. 7). It is well known that the absorption coefficient of an amorphous semiconductor has a characteristic relation [36]:

$$(\alpha h\nu)^{1/2} = B(h\nu - E_g) \quad (2)$$

in which $h\nu$ is the photon energy, $E_g$ is the apparent optical band gap, $B$ is a constant characteristic of the semiconductor, and $\alpha$ is the absorption coefficient. Therefore, the $E_g$ of the resulted $Ln(OH)_3$ nanorods can be obtained by the extrapolation of the above relation to be 4.25–5.60 eV (see Fig. 7 inset).

To explore the possibilities of luminescent properties by $Ln(OH)_3$ nanorods, we carried out PL measurements at room temperature. The room temperature emission spectrum of $Ln(OH)_3$

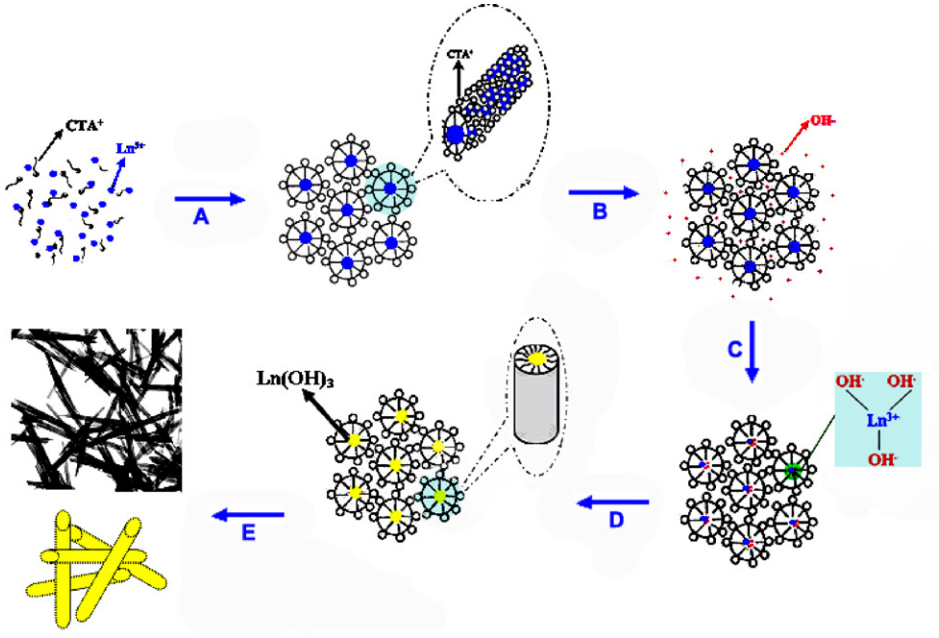


**Fig. 6.** Schematic diagram of the proposed mechanism for the formation of the $Ln(OH)_3$ nanorods in room temperature. (A) Surfactant-inorganic ions interaction, (B) inorganic ions polymerization, (C) inorganic ions–hydroxyl interaction, (D) aging, and (E) washing.

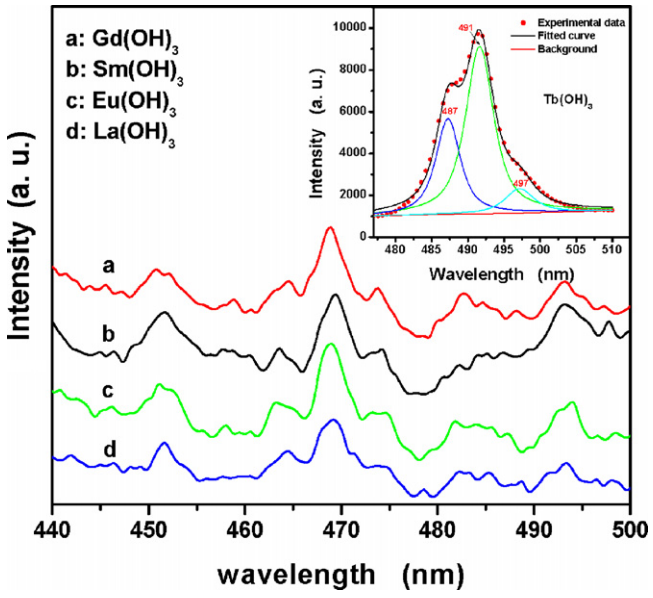


**Fig. 8.** Room temperature photoluminescence spectra of $Ln(OH)_3$ nanorods.

nanorods is shown in Fig. 8. In our investigation, room temperature photoluminescence spectra were performed with an excitation wavelength ($\lambda_{ex}$ = 275 nm). The $^5D_3 \rightarrow {}^7F_j$ ($j$ = 3–6) emission peaks at the wavelength below 500 nm were found in the PL spectra. The strongest emission band was located at 468 nm, which is a typical blue band. $La^{3+}$ has not any luminescence because of the zero electrons in the 4f shell, and La cannot be regarded as an emission center and cannot radiate light from the inner atomic 4f shell when crystalline $La(OH)_3$ is formed [14,37]. The emission of 468 nm could not contribute to the transition from the conduction band to the valence band. The emission does not originate from a transition between the conduction and valence band, while comes from a deep-level or trap-state emission. The morphology of the nanorods suggests that they play a major role in the emission origination. The similar results can be found in reference reported by Wang and co-workers [14]. The trivalent lanthanide ions (Sm, Tb, Eu, and Gd) hold a special place in photonics because of their unique photophysical properties, especially with respect to the generation and amplification of light. A lot of work on luminescent materials based on lanthanide ions is about finding ways to introduce these ions into a material while keeping the ions brightly luminescent and the material intact. However, the O–H vibrations of water are good quenchers of lanthanide luminescence. Many of the efforts in the development of luminescent lanthanide complexes are aimed at protecting the ion from these quenchers, and thus enable luminescence in aqueous media. Lanthanide hydroxides have not any luminescence. In our case, the samples exhibited the emission peaks of room temperature photoluminescence. Especially, the $Tb(OH)_3$ nanorods displayed green emission with the strongest narrow bands at 491 nm corresponding to the intra-4f transitions $^5D_4 \rightarrow {}^7F_6$ [38,39]. We think it is same as the $La(OH)_3$ nanorods discussed above. The morphology of the nanorods plays a major role in the emission origination. Further work is to be done to get a definite understanding.

## 4. Conclusions

In summary, we found a simple route to prepare $Ln(OH)_3$ nanorods by a facile process with use of CTAB as a template agent at room temperature. It is considered that this simple aqueous solution synthetic route can be applied as a general method for the preparation of rare-earth hydroxides with 1D nanostructures. $Ln(OH)_3$ nanorods were analyzed by XRD, FTIR, TEM, Raman spectroscopy, and photoluminescence measurements. The results showed that the stable, crystalline pure hexagonal phase $Ln(OH)_3$ one-dimensional rod-like nanostructures with diameters of approximately 10–30 nm and lengths of 150–500 nm were obtained. The samples also exhibited room temperature photoluminescence of four emission peaks at the wavelength below 500 nm, respectively.

## Acknowledgement

This work was supported by Graduate Research Project of Yunnan University, China (no. ynuy200935).

## References

[1] J.T. Hu, T.W. Odom, C.M. Lieber, Acc. Chem. Res. 32 (1999) 435–445.
[2] G.Y. Adachi, N. Imanaka, Chem. Rev. 98 (1998) 1479–1514.
[3] A.W. Xu, Y. Gao, H.Q. Liu, J. Catal. 207 (2002) 151–157.
[4] A.H. Peruski, L.H. Johnson, L.F. Peruski, J. Immunol. Methods 263 (2002) 35–41.
[5] J.A. Capobianco, J.C. Boyer, F. Vetrone, A. Speghini, M. Bettinelli, Chem. Mater. 14 (2002) 2915–2921.
[6] J. Dhanaraj, R. Jagannathan, T.R.N. Kutty, C.H. Lu, J. Phys. Chem. B 105 (2001) 11098–11105.
[7] S. Daniele, L.G. Hubert-Pfalzgraf, J. Sol–Gel Sci. Technol. 35 (2005) 57–64.
[8] C.S. Xu, Y.F. Zheng, Y. Wang, Mater. Res. Bull. 43 (2008) 1106–1111.
[9] C.R. Patra, R. Bhattacharya, S. Patra, N.E. Vlahakis, A. Gabashvili, Y. Koltypin, A. Gedanken, P. Mukherjee, D. Mukhopadhyay, Adv. Mater. 20 (2008) 753–756.
[10] G. Jia, K. Liu, Y.H. Zheng, Y.H. Song, M. Yang, H.P. You, J. Phys. Chem. C 113 (2009) 6050–6055.
[11] N. Zhang, R. Yi, L.B. Zhou, G.H. Gao, R.R. Shi, G.Z. Qiu, X.H. Liu, Mater. Chem. Phys. 114 (2009) 160–167.
[12] B. Tang, J.C. Ge, C.J. Wu, Nanotechnology 15 (2004) 1273–1276.
[13] Y.D. Yin, G.Y. Hong, Chinese Chem. Lett. 16 (2005) 1659–1662.
[14] C.G. Hu, H. Liu, W. Dong, Y.Y. Zhang, G. Bao, C.S. Lao, Z.L. Wang, Adv. Mater. 19 (2007) 470–474.
[15] S.G. Dixit, A.R. Mahadeshwar, S.K. Haram, Colloid. Surf. A: Physicochem. Eng. Aspect 133 (1998) 69–75.
[16] Z.H. Xu, C.X. Li, P.P. Yang, Z.Y. Hou, C.M. Zhang, J. Lin, Cryst. Growth Des. 9 (2009) 4127–4135.
[17] X. Wang, Y.D. Li, Inorg. Chem. 45 (2006) 7522–7534.
[18] M. Huang, S. Mao, H. Feick, H. Yan, Y. Wu, H. Kind, E. Weber, R. Russo, P.D. Yang, Science 292 (2001) 1897–1899.
[19] G. Zou, R. Liu, W. Chen, Z. Xu, Mater. Res. Bull. 42 (2007) 1153–1158.
[20] Q. Tang, Z. Liu, S. Li, S. Zhang, X. Liu, Y. Qian, J. Cryst. Growth 259 (2003) 208–214.
[21] K.L. Wong, G.L. Law, M.B. Murphy, P.A. Tanner, W.T. Wong, P.K.S. Lam, M.H.W. Lam, Inorg. Chem. 47 (2008) 5190–5196.
[22] X.Y. Ma, H. Zhang, Y.J. Ji, J. Xu, D. Yang, Mater. Lett. 58 (2004) 1180–1182.
[23] Z.W. Wang, L.L. Daemen, Y.S. Zhao, C.S. Zha, R.T. Downs, X.D. Wang, Z.L. Wang, R.J. Hemley, Nat. Mater. 4 (2005) 922–927.
[24] M.B. Salem, B. Yangui, G. Schiffmacher, C. Boulesteix, Phys. Status Solidi A 87 (1985) 527–536.
[25] H. Cölfen, M. Antonietti, Angew. Chem. Int. Ed. 44 (2005) 5576–5591.
[26] K. Ahrenst, H. Gerlinger, H. Lichtblau, G. Schaack, G. AbstreiterS, S. Mroczkowski, J. Phys. C: Solid St. Phys. 13 (1980) 4545–4900.
[27] S.S. Chan, A.T. Bell, J. Catal. 89 (1984) 433–441.
[28] L.M. Cornaglia, J. Múnera, S. Irusta, E.A. Lombardo, Appl. Catal. A: Gen. 263 (2004) 91–101.
[29] T.T. Huong, T.K. Anh, L.Q. Minh, J. Phys.: Conf. Ser. 187 (2009) 012064.
[30] Y.N. Xia, P.D. Yang, Y.G. Sun, Y.Y. Wu, B. Mayers, B. Gates, Y.D. Yin, F. Kim, H.Q. Yan, Adv. Mater. 15 (2003) 353–389.
[31] M. Li, H. Schnablegger, S. Mann, Nature 402 (1999) 393–395.
[32] S. Kwan, F. Kim, J. Arkana, P.D. Yang, Chem. Commun. (2001) 447–448.
[33] Y.Y. Yu, S.S. Chang, C.L. Lee, C.R.C. Wang, J. Phys. Chem. B 101 (1997) 6661–6664.
[34] M.A. El-Sayed, Acc. Chem. Res. 34 (2001) 257–264.
[35] I. Djerdja, G. Garnweitner, D.S. Su, M. Niederberger, J. Solid State Chem. 180 (2007) 2154–2165.
[36] G. Mill, Z.G. Li, D. Meisel, J. Phys. Chem. 92 (1988) 822–828.
[37] J.Y. Li, Luminescent Materials of Rare Earths and Their Applications, Chemical Industry, Beijing, 2003.
[38] F.S. Liu, W.J. Ma, Q.L. Liu, J.K. Liang, J. Luo, L.T. Yang, G.B. Song, Y. Zhang, G.H. Rao, Appl. Surf. Sci. 245 (2005) 391–399.
[39] F. Tao, Z.J. Wang, L.Z. Yao, W.L. Cai, X.G. Li, Nanotechnology 17 (2006) 1079–1082.